An *ab initio* characterization of the electronic structure of $LaCo_xFe_{1-x}O_3$ for $x \leq 0.5$

Dawn L. Geatches, Sebastian Metz,
David N. Mueller and Jennifer Wilcox

Published version information

This is the peer reviewed version of the following article:

Citation: DL Geatches et al. "An *ab initio* characterization of the electronic structure of $LaCo_xFe_{1-x}O_3$ for $x \leq 0.5$." Physica Status Solidi B, vol. 253, no. 9 (2016): 1673-1687.

DOI: 10.1002/pssb.201600141

Which has been published in final form at 10.1002/pssb.201600141. This article may be used for non-commercial purposes in accordance With Wiley-VCH Terms and Conditions for self-archiving.

Please cite only the published version using the reference above. This is the citation assigned by the publisher at the time of issuing the AAM. Please check the publisher's website for any updates.

pss-Header will be provided by the publisher

An *ab initio* characterization of the electronic structure of $LaCo_xFe_{1-x}O_3$ for $x \leq 0.5$

Dawn L. Geatches[*,1], Sebastian Metz[1], David N. Mueller[2], and Jennifer Wilcox[3]

[1] Scientific Computing Dept., STFC Daresbury Laboratory, Warrington, WA4 4AD, UK
[2] Forschungszentrum Jülich, Peter Grünberg Institute, (PGI-6), Walter-Johnen-Str., 52425 Jülich, Germany
[3] Dept. Energy Resources Engineering, 367 Panama Street, Stanford University, CA 94305, USA

Received ZZZ, revised ZZZ, accepted ZZZ
Published online ZZZ (Dates will be provided by the publisher.)

Keywords. $LaCo_xFe_{1-x}O_3$, DFT calculations, PDOS, spin states, charge analysis

* Corresponding author: dawn.geatches@stfc.ac.uk, Phone: +44 1925 603667

Solid oxide fuel cells are an important class of energy conversion devices in the search to replace fossil fuels. Their electrodes' materials mostly belong to the perovskite family, which in their versatile composition are numerous; here we focus on the perovskite $LaCo_xFe_{1-x}O_3$ and examine its electronic structure for $x \leq 0.5$ using density functional theory with a plane wave basis and pseudopotentials. The resulting lattice parameters show good agreement with experiment, and the Mulliken and Bader charges show that iron and cobalt mostly remain as Fe^{3+} and Co^{3+} throughout an increasing Co:Fe ratio. The charge and spin magnitudes of oxygen ions is determined by their local, cation neighbours with the largest charge and spin magnitudes found on oxygen ions sandwiched between two Fe ions. Density of states and partial density of states analyses reveal that increasing the ratio of Co to Fe in oxygen stoichiometric materials decreases their relative, semi-conducting nature towards insulating, by virtue of the decrease in the number of (conducting) O-Fe-O bonds and the increase in (insulating) O-Co-O bonds. The appearance of an intermediate spin state of Co and examination of its PDOS confirms the hypothesis that Co-O, d-p hybridization is a necessary factor for its occurrence.

1 Introduction Oxides of the perovskite type with the general formula ABO_3 can accommodate (Alkaline) Earth and Lanthanide elements on the A site, and virtually the whole range of transition metals on the B-site, leading to a wide range of chemical versatility [1]. The use of substitutions and different formal oxidation states allow fine tuning of the electrochemical activity, important in redox reactions as utilized in electrolysers [2], catalytic conversions [3,4], and fuel cells. They produce a large number of candidate compounds especially for use in solid oxide fuel cells (SOFC) as cathode materials [1, 5,6].

The redox chemistry of a material is governed by its band structure and the accessible states at the Fermi level during oxidation/reduction [7]. Judicious choice of late 3d transition metals enables the engineering of a perovskite-based material towards the efficacy required for a specific reaction, for an increasing number of different applications [8].

The properties and reactivity of ABO_3 perovskites, have been, and continue to be, explored extensively experimentally, see for example the reviews of Tejuca et al.[9], Johnsson and Lemmens [10], Jiang [11], Kilner [12], Kuklja et al.[13], and a recent review of perovskites for photocatalytic applications [14] and the references therein. Computational, *in silico* experiments are also prevalent in this field, with the current literature dominated by studies into the energy of formation of cationic and anionic defects [5, 15-17]; the migration and conductivity of oxygen defects [18-24]; activation energies of oxygen vacancy migration [25] and the driving design principles of their formation [26]; characterization of defect behavior [27], and more recently, multi-scale simulations of oxygen migration [28]. The common theme of these investigations is oxygen vacancies, which are intrinsic to the behavior of SOFCs; they can be created by substitutions on the A site with ions of a lower oxidation state, e.g. Sr^{2+} replacing La^{3+}, resulting in $La_{1-y}Sr_yBO_{3-\delta}$. Additional versatility can be obtained by substitutions of the same oxidation state on the B site (B1/B2 substitutions), e.g. Co^{3+} replacing Fe^{3+}, resulting in $La_ySr_{1-y}Co_xFe_{1-x}O_{3-\delta}$.

The cathode of a SOFC catalyses the oxygen reduction reaction, (ORR) i.e. the conversion of O_2 (gas) to $2O^{2-}$ (bulk). The generated O^{2-} will occupy one of the oxygen vacancies

at the surface of the cathode material and then migrate through the cathode to the electrolyte.

The important role of the migration of oxygen (as O^{2-}) and its vacancies explains the prevalence of computational work in this area. The vacancies however, do not exist in isolation; the electronic structure of an oxygen ion positioned between two cobalt ions is different to that of an oxygen ion positioned between two iron atoms, and to that between cobalt and iron. Therefore, by understanding the electronic structure of the pure materials and the effect of B1/B2 substitutions in the absence of oxygen vacancies it should be possible to fundamentally understand the effects of the component characteristics comprising SOFCs, enabling their design for specific attributes.

In the current literature there seems to be an absence of published computational studies exploring the effect of the B1/B2 substitution ratio on the oxygen vacancies, energies and migration, which is not surprising given that it would be computationally infeasible to take account of all of the relevant variables within a single study. Rather, the emphasis has been on the effect of A-site substitutions on the formation and migration of oxygen vacancies [29-31], as well as exploring the effect of the oxygen vacancies on the electronic properties of perovskite-like materials [32]. The problem would be more tractable if the underlying B1/B2 substitution ratio trends were understood and the corresponding models were then used as templates for the creation of cation/anion vacancies, which provides the motivation for the work we present here.

In particular, we are focusing on $LaCo_xFe_{1-x}O_3$ due to its versatility and varied applications such as a perovskite-based catalyst for the total oxidation of methane [33] and as a catalytic precursor for the production of syngas [34]. Also, $LaCo_xFe_{1-x}O_3$ is used in the catalytic decomposition of N_2O at high temperatures [35], is the cathode material for intermediate temperature SOFCs [36], and, as a double perovskite (La_2CoFeO_6) has recently been reported as having photocatalytic properties [37]. In addition, it is a precursor of $La_ySr_{1-y}Co_xFe_{1-x}O_{3-\delta}$ used in the steam-reforming of ethanol to produce hydrogen [38].

In this work we model different arrangements of a range of ratios of cationic substitutions of Co and Fe to determine the importance of the effects of the local ionic environment on O, Co and Fe. Understanding such effects lays the foundations for larger-scale modelling, such as the diffusion of oxygen vacancies through the solid oxide fuel cell cathode material, $La_ySr_{1-y}Co_xFe_{1-x}O_{3-\delta}$. Also, understanding the effect of an increasing ratio of Co to Fe in $LaCo_xFe_{1-x}O_3$ provides insight into the experimental observations described in the literature such as the various spin and oxidation states found in this group of materials. It is important to note here that this study aims to elucidate the respective intrinsic bonding environments of O as a function of Fe and Co coordination, free of extrinsic effects such as aliovalent doping at the A-site or oxygen exchange with the surrounding atmosphere.

The following provides the details of the eight, (initially) cubic models of $LaCo_xFe_{1-x}O_3$ where x = 0, 0.125, 0.25, 0.375, 0.5, and analyses of their electronic structures post relaxation of their atomic coordinates, which includes lattice lengths, charges, spins, density of states (DOS) and partial density of states (PDOS). We compare our computational results to experimental results where applicable.

2 Computational and Model Details

Perovskites are found in rhombohedral, orthorhombic and cubic symmetries [10, 18], the latter is believed to be prevalent at both room temperature and high operating temperatures [15, 39]. One experimental study into the crystal structure and magnetic properties of $LaCo_{1-x}Fe_xO_{3-\delta}$ [40], found for $0.15 < x < 0.7$ a mixture of rhombohedral and orthorhombic phases, and another into its electrical conductivity [39] found $LaCo_{0.4}Fe_{0.6}O_{3-\delta}$ to be orthorhombic, although its x-ray diffraction pattern indicated the presence of different phases. The potential complications of different phases appearing with different ratios of Co:Fe has been obviated by adopting cubic symmetry throughout, i.e., the template model was cubic $LaFeO_3$ with a, b, c = 7.94 Å, and α, β, γ = 90°, containing 8-La, 24-O and 8-Fe atoms, corresponding to a Co substitution of zero, i.e., x = 0, and all models are based on this cubic template. For $x \geq 0.5$ in $LaCo_xFe_{1-x}O_3$ a transition to rhombohedral symmetry occurs [41], which is a further complication we have avoided by choosing $x \leq 0.5$.

Substituting one Fe by one Co corresponding to the ratio Co:Fe of 1:7, i.e., x = 0.125 produced $LaCo_{0.125}Fe_{0.875}O_3$ with one permutation of the relative positions of Co to Fe. Substituting two Fe by two Co produced $LaCo_{0.25}Fe_{0.75}O_3$ with three permutations where the Co occupied relative positions equivalent to (0,0,0) and (1,0,0); (0,0,0) and (1,1,0); (0,0,0) and (1,1,1). A pragmatic approach was taken when substituting three and four Fe by Co to reduce the number of permutations to consider, i.e., the lowest energy configuration of $LaCo_{0.25}Fe_{0.75}O_3$ was used as the template for the addition of the third and fourth Co producing $LaCo_{0.375}Fe_{0.675}O_3$ and $LaCo_{0.5}Fe_{0.5}O_3$ respectively. The structure containing three Co was thus chosen in a way that it can be derived from all three models containing two Co. Two of six possible permutations of the 1:1 Co/Fe ratio were chosen, one based on the preceding three-Co model and one corresponding to an alternating Co/Fe pattern modelled in the double perovskite, La_2FeCoO_6 [42]. All models are shown in Fig. 1 together with their labels that are used interchangeably from this point onwards.

Ab initio electronic structure calculations were performed on a set of eight models using the density functional theory (DFT) code, CASTEP [43] employing a plane wave basis set and pseudopotentials within the DFT formalism [44-46].

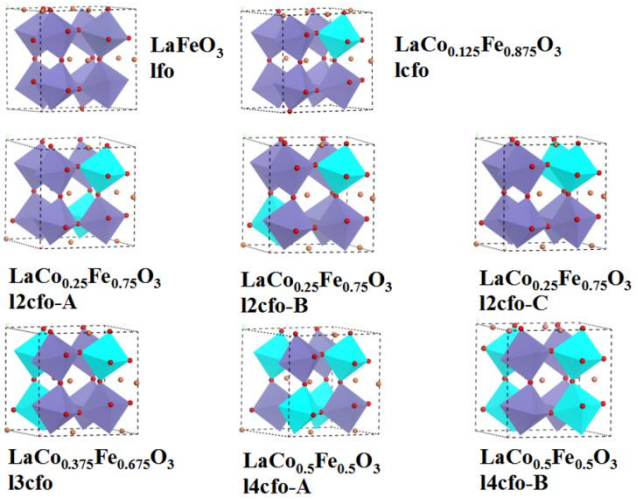

Figure 1 Relaxed models, their formulae and labels. Red - oxygen; purple – iron; blue – cobalt; orange – lanthanum.

The valence electron wavefunctions were expanded in a plane wave basis set represented by a kinetic energy cut-off of 400 eV, which converged energies to less than 0.1meV/atom (using a fine density grid 1.5 times finer than the coarse grid). The electron-ion interactions were described by ultrasoft, Perdew, Burke and Ernzerhof (PBE) pseudopotentials [47, 48] (including core-corrections for Fe and Co [49]), which were consistent with the description of the exchange-correlation effects by the generalized gradient approximation (GGA) density functional, specifically (GGA)PBE [50]. The specific pseudopotentials were: O -2$s^2$2p^4; Fe -3$d^6$4s^2; Co -3$d^7$4s^2; La -5$s^2$5$p^6$5$d^1$6s^2.

For geometry optimization, the Broyden-Fletcher-Goldfarb-Shanno (BFGS) algorithm in its implementation for periodic systems [51] was used in combination with ensemble density functional theory [52]. The Brillouin zone integrations were performed on a Monkhorst-Pack grid [53] of 4 x 4 x 4 k-points, which converged forces to three decimal places. The electronic energy tolerance was 1 x 10^{-8} eV, the energy change per ion per BFGS was converged to 1 x 10^{-5} eV, and the maximum force was converged to at least 0.05 eV/Å. All calculations were spin polarized and the models were created and visualized using Materials Studio [10].

The inclusion of Fe and Co necessitated the inclusion of Hubbard (*U*) parameters due to the inability of (GGA) PBE to describe the strongly correlated d-electrons, which has consequences for many physical quantities including, for example, the effects of the structural and electronic properties of perovskites under pressure [54]. An early LDA + *U* study treated the t_{2g} and e_g electrons of transition metals separately (localized and itinerant respectively) and obtained an appropriate, insulating band structure for La*M*O_3 (*M* = Ti-Cu) [55], validating the need for this additional approximation.

A range of values for both elements currently exist, from 4.0 to 5.4 eV for Fe [15, 26, 56, 57] in $LaFeO_3$ and from 2.5 to 5.85 eV for Co [15, 26, 56-59] in $LaCoO_3$. These were obtained by various theoretical methods from band-gap tweaking to systematically testing a range of *U* and *J* parameters and comparing the resulting magnetic moments, optical and photoemission data to those obtained experimentally. We have been unable to find a study involving a range of Fe:Co ratios in the La*M*O_3 (i.e., *M* = Fe and Co) perovskites and therefore do not have Hubbard parameters for Fe and Co in this environment, however, as we are testing a range of models with increasing doping of Co we have chosen values from the ranges cited and kept them fixed in all models. In particular, we chose those derived from ab initio methods using exact exchange and Coulomb integrals in unrestricted Hartree-Fock calculations, that were then related to the *U* and *J* parameters in DFT + *U* calculations, producing U_{eff} = 4.3 eV for Fe and U_{eff} = 4.0 eV for Co (where here, U_{eff} = *U* - *J*) [26, 60, 61]. Including Hartree Fock exchange appears to give reliable valence and conduction band d-states, according to a DFT+*U* study of α-Fe_2O_3 that used different percentages of Hartree Fock exchange. Comparing their results with X-ray adsorption near edge spectra, (XANES) they found that both the theoretical and experimental valence and conduction band occupations matched.

The energetically lowest lying spin states of $LaCoO_3$ are elusive and difficult to determine experimentally as they vary with temperature between low, intermediate and high spins of Co [58, 62-64]. For barium/strontium ferrate/cobaltate (BSCF) [28] these spin states could be reproduced using DFT+*U* [59] by including spin-orbit coupling [58], for $LaCoO_3$, however, the pragmatic approach of enforcing the ferromagnetic spin state has been reported [15]. An experimental study of the crystal structure and magnetic properties of $LaCo_xFe_{1-x}O_3$ found that structures containing more than 40% iron exhibited weak spontaneous magnetization, which was explained as Co^{3+} ions being in a low spin state [40]. Clearly, the spin state of a particular configuration of $LaCo_xFe_{1-x}O_3$ corresponding to that found experimentally is difficult to know in advance. Test calculations gave the lowest energy configurations when no spin constraints were imposed, hence this is the method applied in this work. This approach is justified computationally because the same parameters are applied to all models, with the only variables being the ratio of Fe:Co and their arrangements.

Following full relaxations of the lattice and ions to the convergence criteria described above, the charge density of the models was analysed using Mulliken, [65] and topological, Bader population analysis [66-68]. Mulliken population analysis in CASTEP is implemented by first projecting the plane wave states onto a localized basis [69], and then analyzing these projected states by the Mulliken formalism to produce a population analysis [70-72].

Mulliken analysis is particularly useful for identifying trends in consistently-parametrized systems [73] and not for calculating absolute charges due to its sensitivity to the atomic basis set [74]. We have included them for two reasons, firstly to identify trends in the charges and secondly to provide them for other researchers who may wish to use them to parameterize force-fields for larger-scale modelling. Topological charge analysis calculates charges by partitioning the electron density into volumes defined by regions of low charge density, which typically lie between atoms, and integrating the enclosed electron density to obtain atom-centered charges. Obtaining the same trends from two different population and charge analysis methods for the effect of substituting $LaFeO_3$ with Co, strongly supports the validity of the provided conclusions.

3 Results and discussion

3.1 Results

3.1.1 Lattice parameters Figure 1 shows the relaxed models, their formulae and labels used throughout this study, and Table 1 reports their parameters together with experimental and computational data from the literature. Following relaxation of l2cfo-A, the resulting lattice parameters were fixed and used for l2cfo-B and l2cfo-C, whereas for l3cfo, l4cfo-A, -B, all lattice parameters were allowed to relax. The variation of less than 1% seen in the relaxed geometries of the latter confirms that both approaches are acceptable. Most of the reported experimental values in Table 1 report lattice parameters for orthorhombic unit cells, whereas the simulations exploit the symmetry of cubic unit cells. Converting a = 5.56 Å (a lattice parameter of $LaFeO_3$ Wu et al. [35]) from orthorhombic to a 2x2x2 cubic unit cell as used in this work gives 7.86 Å agreeing with the simulated value to within 2%. The available experimental data do not exactly match the Co:Fe ratio of the simulations, but were chosen for their close match. The trends prevailing within the two sets of data are the same, namely the substitution of Fe by Co causes a reduction in the lattice lengths by less than 2%, which confirms the suitability of the choice of the GGA(PBE) exchange correlation functional as well as the Hubbard parameters, at least from a geometrical perspective.

3.1.2 Charge analysis Substituting Co for Fe in $LaFeO_3$ creates different bonding groups, where the term 'bonding' describes a series of nearest neighbour ions. For example, in $LaFeO_3$ there are only Fe-O nearest neighbours such that every oxygen is linearly coordinated to two iron cations. If one cobalt ion is substituted by one iron ion to produce $LaCo_{0.125}Fe_{0.875}O_3$ another grouping appears, oxygen sandwiched between iron and cobalt. The substitution of more than one iron by cobalt could introduce one more nearest neighbour grouping - that of oxygen sandwiched between two cobalts. The following notation is used throughout the remainder of this study to describe these nearest neighbor 'bonding' groups: OFF means the oxygen between two irons; OFC means the oxygen between cobalt and iron; OCC means the oxygen between two cobalt cations (shown in Fig. 2).

Table 2 shows the average Bader charges for each model. The Mulliken charges are given in Fig. S1 (in the Supplementary Information) and show the same trends as the Bader charges. The results of Pavone et al.[26] found DFT+U simulations gave Bader charges in defect-free $LaFeO_3$ of La: 2.08, Fe: 1.71, O: -1.26. The differences between the Bader charges found in this study (La: 2.17, Fe: 1.57 and 1.78, O: -1.30) and Pavone's could be due to the different anti-ferromagnetic (AFM) configurations found, where the latter report that the Fe have high-spin configurations with a preference for AFM coupling between neighbouring Fe cations. The AFM configuration we found (Fig. 3) has two of the eight Fe with lower spin magnitudes of 3.14 and correspondingly lower charges, resulting in an overall average charge for Fe of 1.67. Nevertheless, both studies agree in their descriptions of $LaFeO_3$ as being AFM overall with a net magnetization of zero exhibited by the DOS (Fig. 4).

Their defect-free $LaCoO_3$, gives charges of La: 2.07, Co: 1.41 and O: -1.16. We can use these values to compare them to the OCC groups appearing in l4cfo-B, with charges of La: 2.17, Co: 1.38 and O: -1.19. Both studies agree in the relative values of La, Co and O and with the general trend that the introduction of Co lowers the magnitude of oxygen's charge, and that Fe has a higher charge than Co. Both Table 2 and Fig. 3 (Bader charges and spins) show that increasing the Co:Fe ratio has no effect on the charge of Fe nor Co, and the latter has a consistent charge except in the case of l4cfo-A where it is also 1.6. As that charge does not appear in l4cfo-B it therefore cannot depend on the number of Co, but rather their relative coordination. This can be explained by the

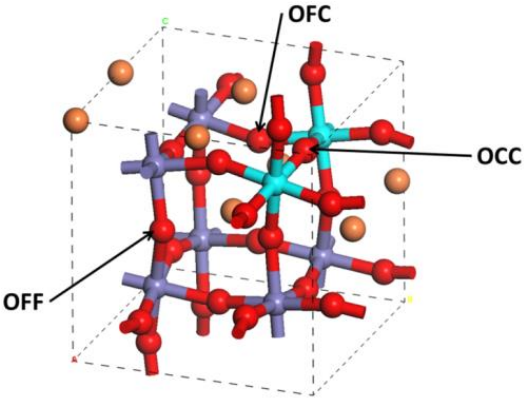

Figure 2 Labels describing nearest neighbour oxygen bonding groups, e.g., OFF means the oxygen located between two Fe cati ons; OFC the oxygen between Fe and Co; OCC the oxygen between two Co cations.

Model	*a*	*b*	*c*	α	β	γ
$LaFeO_3$	8.01	8.03	8.00	89.9	89.9	90.2
$LaFeO_3$-sim[15]	7.88	7.88	7.88	90	90	90
(*U*:4.0/6.0 eV)	3.94	3.94	3.94			
$LaFeO_3$-exp[63]	7.85	7.85	7.85	90	90	90
$LaFeO_3$-exp[35]	7.86	7.86	7.86	90	90	90
	5.56	5.56				
$LaFeO_{3-\delta}$-exp[39]	7.86	7.86	7.86	90	90	90
	5.56	5.56				
$LaCo_{0.125}Fe_{0.875}O_3$	7.99	7.95	7.93	89.5	90.4	89.0
$LaCo_{0.125}Fe_{0.875}O_{3-\delta}$-exp[39]	7.83	7.83	7.84	90	90	90
	5.54	5.54				
$LaCo_{0.25}Fe_{0.75}O_3$-A	7.94	7.94	7.95	89.9	90.3	89.0
$LaCo_{0.25}Fe_{0.75}O_3$-B	7.94	7.94	7.95	89.9	90.3	89.0
$LaCo_{0.25}Fe_{0.}75O_3$-C	7.94	7.94	7.95	89.9	90.3	89.0
$LaCo_{0.2}Fe_{0.8}O_3$-exp[35]	7.78	7.82	7.81	90	90	90
	5.50	5.53				
$LaCo_{0.2}Fe_{0.8}O_{3-\delta}$-exp[39]	7.81	7.82	7.81	90	90	90
	5.52	5.53				
$La_{0.6}Sr_{0.4}Co_{0.2}Fe_{0.8}O_{3-\delta}$-exp[38]	7.78	7.86	7.84	90	90	90
	5.50	5.56				
$LaCo_{0.3}Fe_{0.7}O_{3-\delta}$-exp[39]	7.79	7.82	7.80	90	90	90
	5.51	5.53				
$LaCo_{0.375}Fe_{0.675}O_3$	7.96	7.95	7.89	89.3	90.3	89.1
$LaCo_{0.4}Fe_{0.6}O_3$-exp[35]	7.74	7.76	7.77	90	90	90
	5.47	5.49				
$LaCo_{0.42}Fe_{0.58}O_3$-exp[41](4.2 K)	7.78	7.72	7.74	90	90	90
	5.50	5.46				
$LaCo_{0.42}Fe_{0.58}O_3$-exp[41](400 K)	7.81	7.75	7.76	90	90	90
	5.52	5.48				
$LaCo_{0.5}Fe_{0.5}O_3$-A	7.88	7.88	7.85	89.7	90.0	89.0
$LaCo_{0.5}Fe_{0.5}O_3$-B	7.89	7.89	7.84	89.8	90.2	89.0
$La_{0.6}Sr_{0.4}Co_{0.5}Fe_{0.5}O_{3-\delta}$-exp[38]	7.74	7.81	7.76	90	90	90
	5.47	5.52				
$LaCo_{0.5}Fe_{0.5}O_3$-exp[41](6 K)	7.76	7.69	7.70	90	90	90
	5.49	5.44				

Table 1 Relaxed lattice parameters from simulations ('sim') and experiments ('exp') in Å and degrees. Most experimental data were for the orthorhombic unit cell (bottom entries per row) which we converted to a cubic unit cell (top entries per row). The cited simulated data (for $LaFeO_3$-sim) were from a cubic unit cell half the size (lower) of the unit cells we used (top). The range of Hubbard parameters used in the cited work is denoted by *U*.

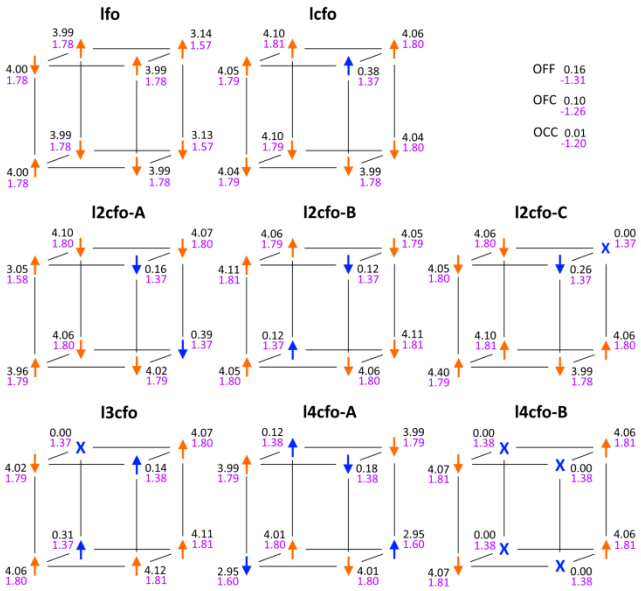

Figure 3 Bader charges (purple text) and spin magnitudes (black text) of Fe (orange) and Co (blue) and oxygen (top right- average for all systems) in its different bonding groups. Crosses indicate zero spin.

fact that $La(Co,Fe)O_3$ are charge transfer materials, where the O2p-Co/Fe3d charge transfer energy is less than the exchange and Coulomb interaction energy between the d-electrons, denoted respectively as Δ and U_{dd} by Zaanen et al. [75]. It appears that in the case of Co and Fe the difference between Δ and U_{dd} is smaller for Co, leading to an increased transfer of charge from O to Co.

The low charge Co are surrounded by six Fe as next-nearest neighbours, four of them with the same spin orientation, two with opposite spin orientation. The high charge Co are surrounded by six Fe, four of them with the opposite spin orientation, two with the same orientation, see Fig. 3. l4cfo-A is the only model in the set of eight systems with no OFF bonding groups, which might also contribute to the low charge of Co.

Where there are only OFF groups the oxygen ions have a consistent charge of -1.30, where OFC groups exist they have a charge of -1.25/-1.26, except in the case of l4cfo-A where they range from -1.26 to -1.30, and where OCC groups appear the oxygen ions have a charge of -1.19/-1.20.

Model	Fe-c	Fe–s	Co-c	Co-s	OFF-c	OFF-s	OFC-c	OFC-s	OCC-c	OCC-s
$LaFeO_3$	1.57	3.14	-	-	-1.30	0.02	-	-	-	-
	1.78	3.99								
$LaFeO_3$[26](U:4.3 eV)	1.71	4.21	-	-	-1.26					
$LaFeO_3$[63]	-	4.00	-	-	-	-	-	-	-	-
$LaFeO_3$[5] (U:4.0 eV)	-	4.00	-	-	-	-	-	-	-	-
$LaFeO_3$[76](U:5.4 eV)	-	4.23[a]	-	-	-	-	-	-	-	-
		4.06[b]								
$LaCo_{0.125}Fe_{0.875}O_3$	1.80	4.05	1.37	0.38	-1.32	0.00	-1.26	0.08	-	-
$LaCo_{0.25}Fe_{0.75}O_3$-A	1.79	4.04	1.37	0.16	-1.25	0.02	-1.25	0.09	-	-
	1.58	3.05	1.37	0.39	-1.31	0.12				
$LaCo_{0.25}Fe_{0.75}O_3$-B	1.80	4.07	1.37	0.16	-1.32	0 to	-1.25	0.12	-	-
			1.37	0.39		0.24				
$LaCo_{0.25}Fe_{0.75}O_3$-C	1.80	4.05	1.37	0.00	-1.31	0.12	-1.26	0.10	-1.20	0.01
			1.37	0.26						
$LaCo_{0.375}Fe_{0.675}O_3$	1.80	4.08	1.38	0.14	-1.32	0 to	-1.26	0.11	-1.19	0.01
			1.37	0.31		0.25				
			1.37	0.00						
$LaCo_{0.5}Fe_{0.5}O_3$-A	1.80	4.00	1.38	0.12	-	-	-1.26	0.02	-	-
			1.38	0.18			-1.27	to		
			1.60	2.95			-1.28	0.20		
			1.60	2.95			-1.30			
$LaCo_{0.5}Fe_{0.5}O_3$-B	1.81	4.06	1.38	0.00	-1.32	0.24	-1.26	0.12	-1.19	0.00
$LaCo_{0.5}Fe_{0.5}O_3$[41]	-	3.2	-	Low						
$LaCoO_3$[26](U:4.0eV)	-	-	1.41	1.49	-	-	-	-	-1.16	

Table 2 Average Bader charges (-c) and spin magnitudes (-s) of Fe, Co and O (in different bonding groups as defined in Figure 1b) for each of the model systems shown and labelled in Figure 1a. Columns 7 and 9 show the maximum and minimum spin magnitudes (denoted by inclusion of 'to' where there were ranges of values). The average Bader charge of La was 2.17 for all models in this study. Spins are in units of μB, charges in units of +e and 'U' is the Hubbard parameter used in the cited computational studies. [a] refers to FM and [b] to AFM (G-type).

As the number of OFF groups decreases that oxygen's charge generally decreases slightly to -1.31/-1.32 and in the case of l2cfo-A increases to include two instances of -1.25, explained by the appearance of two low spin, low charge Fe. This generally shows that the introduction of Co does not only affect the neighbouring O, but has a long-range effect extending to Fe and then the O next to these Fe, which should be expected for these materials involving both charge transfer and correlated d-electrons. In other words, the introduction of Co impacts the material as a whole, which gives an indication of why even low doping levels can change the material's properties significantly.

3.1.3 Spins Table 2 also gives the magnitude of the spins; that of Fe is mostly high at approximately 4 μB with two occurrences of approximately 3 μ_B in lfo and l2cfo-A, and although a spin of about 3.2 μ_B was identified experimentally [41], this was in $LaCo_{0.5}Fe_{0.5}O_3$ at 6 K assuming a low spin state for Co^{3+}. The more commonly identified magnetic moment of Fe^{3+} in these lanthanum cobaltate systems is about 4 μ_B, seen experimentally [63] and simulated [5, 76] (U = 4.0 and 5.4 eV, in the respective references) in $LaFeO_3$, and between 3.7 to 4.3 μ_B in $La_{0.875}Sr_{0.125}FeO_{3-\delta}$ and $La_{0.5}Sr_{0.5}FeO_{3-\delta}$ using a range of hybrid density functionals and two different Hubbard values [77]. The spin of Co ranges from 0 to 0.39 μ_B in all of our models except l4fo-A where it is also 2.95 μ_B on two of the four Co. Experimentally, the magnetic moment of Co^{3+} is mostly speculated on and classified as low [41] (out of 'low, 'intermediate' or 'high') for temperatures below 20 K and only on a light substitution of Co by Ni was an intermediate spin state induced in Co[78].

The magnitude of the spins on the oxygen ions of OFF vary from 0 to 0.25, of OFC from 0.02 to 0.20, and of OCC from 0 to 0.01. In another computational study [76] the magnetic moment of oxygen in $LaFeO_3$ (U = 5.4 eV) was reported as 0.21 μ_B in the ferromagnetic phase and 0.00 μ_B in the AFM phase.

3.1.4 Density of states (DOS) and partial density of states (PDOS) Figure 4 shows the total DOS for all models. With the exception of lfo, l2cfo-A and l2cfo-C which are weakly conducting, all other investigated $LaCo_xFe_{1-x}O_3$ systems are shown to be semi-conducting with a band gap of less than 5 eV.

3.1.4.1 Fe The PDOS of Fe, see Fig. 5, for all species is dominated by the d-orbitals, with major peaks at around -

8eV and +2eV and with only minor contributions of the s- and p-orbitals. Comparing the different structures, the most striking feature is the asymmetry of these peaks for some of the structures, most pronounced in l2cfo-A and l3cfo, which originates from the non-zero magnetization of the wavefunction. Closer scrutiny of the PDOS of Fe (see Fig. S2) shows as well that for lfo, the s- and d- orbitals cross the Fermi level; substituting one Co (lcfo) causes a band gap to open up and the substitution of a second Co induces s- and d- orbitals to cross the Fermi again in l2cfo-A, a slight shift to the left (including p-orbitals) in l2cfo-B, (corresponding to a lateral plane of all up-spin and one of all down-spin –see Fig. 1) and no change in the s-, p- and d-orbitals of l2cfo-C relative to lcfo.

The substitution of a third and fourth Co ion causes the growth in conduction band states of all orbitals in l3cfo and l4cfo-B respectively, relative to lcfo, but not in l4cfo-A, which differs from lcfo only in the shrinking of the amplitudes of d-orbitals.

3.1.4.2 Co The PDOS of Co, see Fig. 6, for all species is dominated by the d-orbitals, with major peaks at around -4.5eV and -1eV below the Fermi level and a broadened peak at around +2eV with a clear band gap. As for Fe, there are only minor contributions of the s- and p-orbitals and a (less pronounced) asymmetry of the positive/negative DOS peaks, again most pronounced in l2cfo-A and l3cfo. Also the slight downward shift for the +2eV peak as seen for Fe can be found again for l2cfo-B.

While there is very little difference between the PDOS of the different structures, l4cfo-A shows two distinct additional peaks at -7eV and -6eV. As l4cfo-A is the only structure containing high spin Co centres, assignment is straightforward. Fig. S3 shows a close-up of the s-, p- and d-orbitals of Co and in lcfo they all contain a band gap; the substitution of a second Co induces a slightly smaller band gap in the p- and d-orbitals of l2cfo-A, a slight shift to the left in the s-, p- and d- valence orbitals of l2cfo-B and a

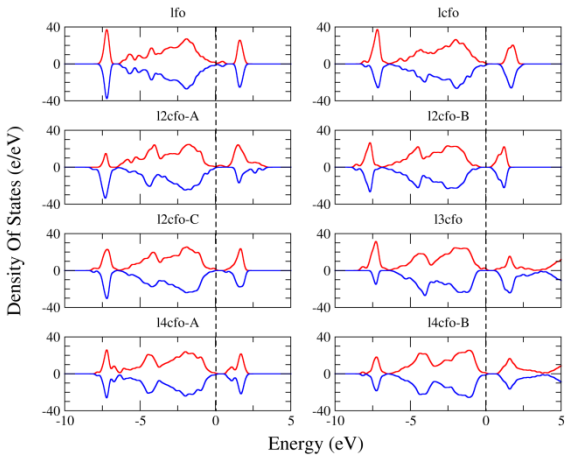

Figure 4 Total Density of states (DOS). Dashed line on this and on all PDOS figures is the Fermi level.

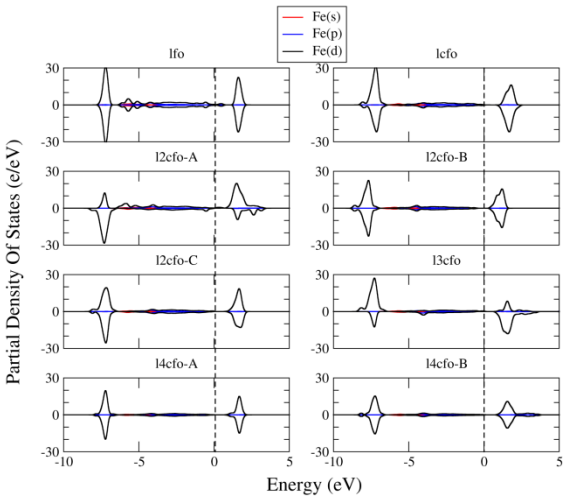

Figure 5 PDOS of Fe.

shift to the left in the s-, p- and d- conduction orbitals of l2cfo-C.

Similar to the effect on the Fe ions, the substitution of a third and fourth Co ion induces an increase and growth in the conduction band states in l3cfo and l4cfo-B respectively, but in l4cfo-A the notable change is the small decrease in band gap compared to lcfo, and slightly smaller band gap than that found in another GGA + *U* exploration of the electronic properties of La_2FeCoO_6 [42].

3.1.4.3 O Figure 7 shows that in all systems the s-orbitals barely change throughout the progressive substitution of Co. The p-orbitals in lfo cross the Fermi level, and substitution of Co results in a separation of the valence and conduction band states in all systems, producing a small band gap.

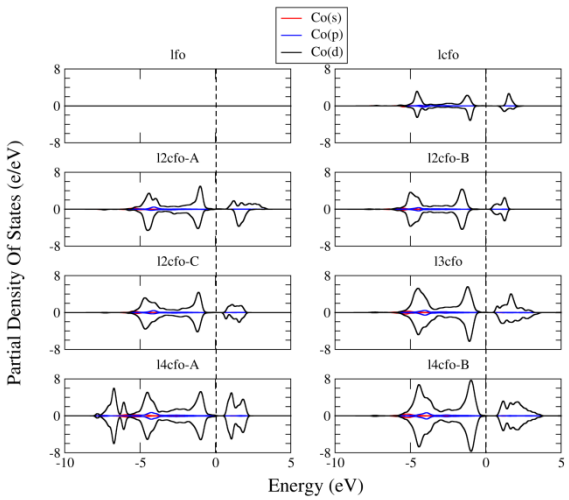

Figure 6 PDOS of Co.

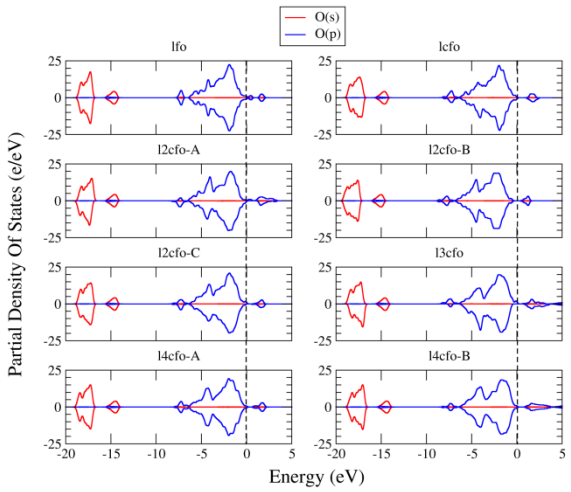

Figure 7 PDOS of O.

Examining the component contributions of OFF, OFC and OCC (Fig. 8) reveals that in all cases of Co ion substitution the p-orbitals of the O ions in the OFF group meet the Fermi level but do not cross it, as do those of the O ions in the OFC group, albeit to a slightly lesser extent, whereas the p-orbitals of the O ions in the OCC group have a slightly larger band gap that extends from below the Fermi level and into the conduction band. The amplitude of the p-orbitals in the conduction bands of l3cfo and l4cfo-B increases for O ions in all three bonding groups, a similar effect to that previously mentioned for Fe and Co ions.

3.1.4.5 La The s- valence orbitals of La are invariant to Co substitution up to three Co, where the inclusion of a fourth Co induces a slight shift towards the Fermi level. Considering the p- and d-valence orbitals of La (Fig. S4) the progressive substitution of cobalt for iron causes the valence states to shift towards the Fermi level on the substitution of one Co and this shift does not change on further substitution of two and three Co. The substitution of a fourth Co for Fe causes a further, smaller shift of the valence states towards the Fermi level. In all cases there are no states at the Fermi level and the conduction band states have an almost undetectable amplitude relative to the valence band states such that they are essentially non-existent, except in l3cfo and l4cfob where s-, p- and d-orbitals appear in the conduction band with amplitudes equivalent to those seen in the valence band.

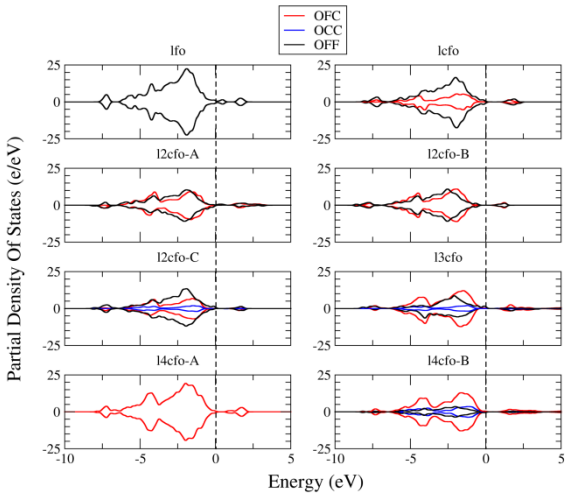

Figure 8 PDOS of O in its different bonding groups.

3.2 Discussion There is good agreement (within 2%) between the experimentally obtained and simulated lattice parameters and both sets show the same trend in decreasing lattice parameters due to the substitution of Fe by Co. The experimental lattice parameters recorded in Table 1 include systems with oxygen vacancies and substitutions of La by Sr, neither of which affects the lattice parameters to a greater extent than does the substitution of Fe by Co – compare for example, the results for $LaCo_{0.2}Fe_{0.8}O_{3-\delta}$ and $La_{0.6}Sr_{0.4}Co_{0.2}Fe_{0.8}O_{3-\delta}$. Similarly, the proportional expansion of the lattice on increasing the temperature is comparable (e.g. $LaCo_{0.42}Fe_{0.58}O_3$ at 4.2K and 400K). This means that we have reproduced the correct experimental trend seen on substituting Fe by Co, and thereby confirmed the appropriateness of the computational parameters. Therefore, the simulated data can be used to explain the relative effects on the electronic structure of an increasing Fe:Co substitution, and these same relative effects (i.e. trends) would be seen in analogous experimental data.

A simple calculation of the energy gained relative to $LaFeO_3$ per Co for Fe substitution, (data shown in Table S1) suggests that most energy is gained on the substitution of one Fe by one Co ion and that additional substitutions gain relatively less energy. For example, at a Co:Fe ratio of 3:5, substituting one Co for one Fe requires 50 meV, similar to the 80 meV found by Kuklja et al. [79], albeit at a Co:Fe ratio of 3:1. To make a more definitive statement on the mixing/demixing behaviour, a full thermodynamic study would be needed. This has been demonstrated to be possible for both the A-sites [80] as well as the B-sites [81], but is beyond the scope of this current study. Additionally, the results of Kuklja et al.'s work [79] showed that mixed A- and B-site disorder (i.e. A-B antisite defects) is energetically unfavourable. Altogether, these results indicate a reduced probability of the growth of isolated islands of Fe and Co, and instead the emergence of a heterogeneous Fe:Co distribution. Within the heterogeneity there could be 'pockets' of specific configurations per Co:Fe substitution ratio, for example, l2cfo-C has the lowest energy of the three configurations of $LaCo_{0.25}Fe_{0.75}O_3$, followed by

l2cfo-B and l2cfo-A with energy differences of 6 meV/atom and 9 meV/atom respectively, which are larger than the energy convergence criterion of 0.1 meV/atom. Therefore, we could infer that within a sample of $LaCo_{0.25}Fe_{0.75}O_3$ the dominant configuration would be l2cfo-C depending on the temperature. Similarly, l4cfo-B has the lower energy of $LaCo_{0.5}Fe_{0.5}O_3$ by 10 meV/atom, so is more likely to be more prevalent than l4cfo-A, but these are only two configurations of six so it is not possible to be definitive about the overall dominant configuration within the scope of this study.

There are clear correlations between the charge and spin of Fe ions across all systems, where a lower charge corresponds to a lower spin. We can use the spin-only magnetic moment $\mu_s = (n(n + 2))^{0.5}$, where n is the number of unpaired electrons, to assign an oxidation state to the Fe. For Fe systems with an even number of electrons (Fe^{2+} and Fe^{4+}) the potential values are μ_s = 0, 2.83 and 4.90. For Fe^{3+} possible values for μ_s are 1.73, 3.87 and 5.92. Given that in most models all Fe ions have a spin magnitude ranging from 3.99 to 4.08 μ_B this corresponds most closely to μ_s =3.87 produced by three unpaired electrons of Fe^{3+}. The two exceptions to this are lfo and l2cfo-A, which have some Fe ions with spin magnitudes of 3.14/3.13 and 3.05 μB respectively. In both models the charge of the lower spin Fe ions is smaller than that of the larger spin Fe ions, ruling out Fe^{4+} as a possible oxidation state, therefore a spin of magnitude ~3 μ_B most closely matches μ_s = 2.83 corresponding to the intermediate spin state produced by two unpaired electrons of Fe^{2+}. The emergence of Fe^{2+} in lfo and l2cfo-A seems random, with two instances in the former and one in the latter, however, closer scrutiny of their local environments explains their appearance. The two low spin Fe in lfo each have four of their six nearest neighbour oxygen ions of the highest (least negative) charge and two (sandwiched between the two Fe) of the lowest (most negative charge), producing an average O ion charge that is more positive than that of those surrounding the higher spin Fe ions. Similarly, the oxygen ion nearest neighbours of the low spin Fe ion in l2cfo-A are all of the highest charge. Therefore, the appearance of the Fe^{2+} ions occurs due to Fe ions gaining electron density from their nearest neighbour O ions.

Repeated calculations of $LaFeO_3$ with imposed symmetry, cubic lattice constraints and looser electronic energy tolerances produced relaxed models with one, three and two lower spin Fe ions respectively, corresponding to half-metallic and two metallic DOS respectively. This means that although the final spin states in $LaFeO_3$ are somewhat sensitive to the computational parameters, the results are variations on a theme, that is, the spins of Fe are either approximately 3 or 4 μB, with corresponding lower and higher charges and their DOS indicate semi-metallic to metallic properties. Experimentally, $LaFeO_3$ is found to be an insulator, and the majority of the theoretical calculations cited in this study report the same where a Hubbard parameter has been used and semi-metallic to metallic where the effective Hubbard parameter is zero [15]. While it is to be expected that different Hubbard parameters will produce different band gaps, where two studies use the same value one might expect to see similar results. The insulating state of $LaFeO_3$ found by Pavone et al. [26] employed the same Hubbard parameter for Fe as we did, and yet we found a semi-metallic state. However, where they used the projected augmented-wave method we use ultrasoft pseudopotentials including nonlinear core corrections for Fe and Co. Where the performance of these two methods has been compared [82] it was shown that the magnetic properties of transition metals (including Fe) were problematic, requiring very accurate augmentation charges. An alternative treatment was found to include the 3p semi-core states as valence states [83]. Exploring the effect of these parameters on the results lies outside the scope of this investigation; suffice it to say that the trends emerging from the series of models we tested are nevertheless robust and self-consistent within the limitations of the parameters used.

It is also worth noting that in Shein et al.'s computational exploration of $LaFeO_3$, two different spin values were identified for Fe, 4.23 and 4.06 μ_B corresponding to the FM and AFM (G-type) configurations [76] respectively. This means that the spin magnitude depends not only on the electron density of the Fe ions, and hence their relative oxidation state, but also on their spin orientations relative to their neighbours, although the latter effect is smaller by a factor of five if the 0.17 μ_B difference of Shein et al.'s results is compared to the difference of 0.85 μ_B of ours for the two different spin values seen in $LaFeO_3$. Our range of relaxed $LaCo_xFe_{1-x}O_3$ mostly exhibit mixed A, C and G - type anti-ferromagnetism with A-type dominating except in $LaCo_{0.5}Fe_{0.5}O_3$-A which is exclusively C-type, behaviour that mirrors the anti-ferromagnetic coupling of neighbouring transition metal cations in SOFC [26]. These AFM properties probably would be lost at operating (i.e. high) temperatures, and like their SOFC cousins they would become paramagnetic at the macroscopic scale [26], with the 1:1, Co:Fe systems losing all magnetic ordering over 360 K [40].

Considering the spin of Co, it appears as zero, low in tenths of μ_B and relatively high at 2.95 μ_B, the latter coinciding with the appearance of higher charge. Following the same analysis as that carried out for Fe ions, we can determine whether there is a corresponding change in oxidation state or a simple electron pairing event. The potential μ_s values for Co^{3+} are 0, 2.83 and 4.90, and for Co^{2+} are 1.73, 3.87 and 5.92. The spin-only magnetic moment closest to the computed value of 2.95 (μB), is μ_s = 2.83 and therefore we conclude that Co^{3+}, unlike Fe^{3+} does not change its oxidation state, but only changes from a low spin state to an intermediate state with two unpaired electrons. This is in agreement with the findings of Pandey et al. [58] who characterise the intermediate spin state of Co^{3+} in $LaCoO_3$ by occupation of the three t_{2g} (d_{xy}, d_{xz}, d_{yz}) by five electrons and single occupation of one of the e_g (d_{xx-yy}, d_{zz}) orbitals, resulting in two of the six d-electrons unpaired.

According to Pandey et al. [58] spin-orbit coupling is important for the intermediate and high spin states of Co^{3+} although the difference with and without it is on the order of hundredths of electron volts. The Hubbard value of Co could also affect the appearance of intermediate and high spin states and ideally, future studies would avoid using the Hubbard parameter altogether and use an environment-independent parameter such as the screened hybrid density functional of Heyd, Scuseria and Ernzerhof (HSE06) [84, 85], which has already proven itself in calculating ($LaTiO_3$) experimentally-predicted Mott insulator, anti- and ferro-magnetic orderings [86]. However, the agreement with the predicted spin-only magnetic moment, μ_s is good enough to confirm that the higher spin corresponds to six d-electrons, with two of them unpaired and hence the oxidation state of Co^{3+} is invariant to the increase in the Fe:Co ratio up to 1:1.

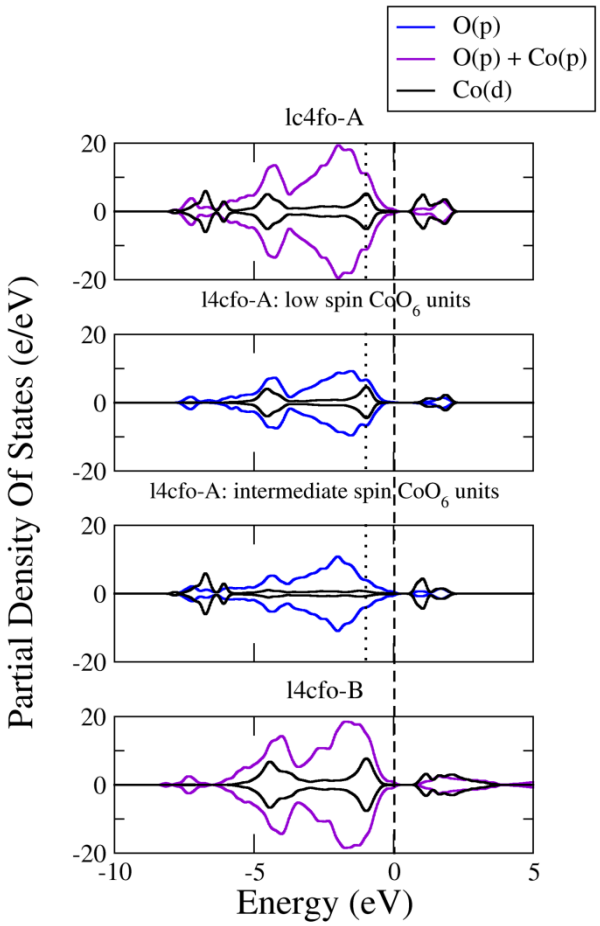

Figure 9 PDOS of O and Co of the two systems containing four Co and four Fe. 'Co-O' unit refers to the nearest neighbour O ions to either the Co of low (0.12/0.18) or intermediate (2.95) spin. i.e. to the respective CoO_6 octahedra. The dashed line marks the Fermi level and the dotted lines indicate the hybridization of Co and O orbitals in l4cfo-A.

On increasing the Co:Fe ratio, no changes are observed for the electronic state of Co^{3+}, except in one case: lc4fo-A, in which there are only OFC groups present, a change from a low spin to an intermediate spin state is seen for two of the four Co^{3+} ions. Tomiyasu et al. [78] showed for $LaCoO_3$ that a low substitution ratio ($LaM_{0.01}Co_{0.99}O_3$) can alter the local spin state of the Co^{3+} ions. While for M=Fe, the experimental substitution ratio (forming far less than one OFC group per CoO_6 octahedron) was too low to observe a switch from low spin to intermediate spin, the 1:1 ratio of Co:Fe (forming six OFC groups per CoO_6 octahedron), according to our calculations, suffices. Korotin et al. [59] discussed in detail the appearance of the intermediate spin state for Co^{3+} in $LaCoO_3$, and reasoned it to be due to the hybridization of the Co, d- (namely the e_g states) and the O, p- states of similar energies. To explore this in closer detail, the PDOS of the O, p- and Co, d- orbitals for l4cfo-A (containing CoO_6 octahedra of low and intermediate spin) and l4cfo-B (containing only CoO_6 octahedra of low spin) are plotted in Fig. 9 (top and bottom graph). The major difference between the two graphs is the appearance of two additional Co, d- peaks at -6.6 eV and -5.9 eV for l4cfo-A. These peaks originate from the intermediate spin CoO_6 octahedra. In addition, the PDOS of the intermediate spin state shows a higher concentration of the Co, d- and O, p- states at the lower end of the conduction band closer to the Fermi level (at about 0.2 eV). None of these Co, d- states, however, find sufficient O, p- states for efficient hybridization. In fact, the PDOS for the low spin CoO_6 octahedra shows much larger PDOS for both Co, d- and O, p- states at -4.5 eV and -1.0 eV, which increases the potential for efficient hybridization.

As the hybridization potential originates from the low spin Co^{3+} ions, one could conclude that this should be even larger in l4cfo-B, where there are more low spin Co^{3+} ions. This is, however, not strictly true, as demonstrated by the distinct shoulder at around -1.0 eV (dotted vertical lines in Fig. 9). This shoulder, coinciding with the Co, d- peak, is only present in l4cfo-A, not in l4cfo-B. We conclude therefore that it takes the presence of the intermediate spin states of the Co^{3+} ions, to enable additional hybridization of the low spin Co, d- states with the O, p- states. As such, our analysis confirms the prediction of Korotin et al. [59] but the latter has to be extended to include the presence of both intermediate and low spin Co^{3+} octahedra. In addition, the presence of mixed low and intermediate spin Co corresponds with their prediction of mixed Co spin states, during the transition from the low to intermediate spin state (that occurs with increasing temperature) [59].

For the intermediate spin state of Co in l4cfo-A a Jahn-Teller distortion is observed: the Co-O bond lengths of the CoO_6 octahedra are split into three pairs of values, with each of the pair of values lying opposite one another,

forming a slightly distorted octahedron. The octahedral bond lengths of the low spin Co of the same system are almost equivalent, forming virtually undistorted octahedra. The Co-octahedra are similarly undistorted in all other systems, which is to expected for d^6 low spin cases. The distortion found for the intermediate spin system could therefore be used as an experimental indicator of the spin state of Co.

Our results suggest that the intermediate spin state of Co can occur when there are sufficient OFC bonding groups. The resulting intermediate spin CoO_6 octahedra are uniquely three-way, asymmetrically distorted. The concurrent presence of low spin Co^{3+} can provide additional stabilization for the intermediate spin state through Co, d-/O, p- hybridization as described above.

Considering the oxygen ions, the magnitude of their spin and charge increases from OCC < OFC < OFF where O ions closest to Fe ions have the largest charge and spin magnitude, and those between two Co ions the smallest, which reflects the relative magnitudes of the spin and charge of the Fe and Co ions. The O ions appear to be influenced by the spin of their nearest neighbour cations, which could explain the increase in magnetic anisotropy seen on the removal of O ions (to create O vacancies) reported in the experimental work of Troyanchuk et al. [40] on $LaCo_{1-x}Fe_xO_{3-\delta}$.

The DOS results of the O ions show that the relative, weakly conducting nature of $LaFeO_3$ is due to the valence electrons in the p-orbitals of the O ions as well as the valence electrons in the s- and d-orbitals of the Fe ions, just crossing the Fermi level. On the substitution of Fe by Co the number of O ions in OFF bonding groups decreases, with an increase in the number of O ions in the OFC and OCC bonding groups, whose valence p-orbitals meet at, and fall short of, the Fermi level respectively, thereby contributing to the formation of a band gap, which persists on further substitution of Co ions. Therefore, there are two contributing factors to the relative, semi-conducting nature of these $LaCo_xFe_{1-x}O_3$ **(**$x \leq 0.5$) materials, the decrease in the number of Fe ions and the decrease in the number of O ions in OFF groups. There appears to be a third contributing factor, the presence of a lower-magnitude spin of the Fe ions, which is observed in $LaFeO_3$ where six of the eight Fe ions have the same spin of magnitude ~ 4 μ_B and two of ~ 3 μ_B, and in $LaCo_{0.25}Fe_{0.75}O_3$-A five Fe have spin of ~ 4 μ_B and one of ~ 3 μ_B resulting in weak conductors in both cases. All other investigated systems are relative semi-conductors with Fe ions of the same spin magnitude (~4 μ_B).

4 Conclusions

We have confirmed that increasing the ratio of Co to Fe in $LaCo_xFe_{1-x}O_3$ materials causes a decrease in the lattice parameters, and have tentatively suggested the growth of regions of specific permutations on increasing Co for Fe substitution. We identified the appearance of Fe as Fe^{2+} in $LaFeO_3$ and $LaCo_{0.25}Fe_{0.75}O_3$(-A), which are intrinsically linked to a lower spin state of Fe, and confirmed that Fe and Co occur mostly as Fe^{3+} and Co^{3+} in these materials. The Bader charge analysis confirmed the greater covalent nature of the Co-O bonds compared to the Fe-O bonds, and both Bader and Mulliken analysis showed that both Fe and Co maintain fairly constant charges throughout an increasing substitution of Fe by Co. The magnitude of the spin and charge of oxygen ions increases from OCC < OFC < OFF where O ions closest to Fe ions have the largest charge and spin magnitude, and those between two Co ions the smallest.

Analysing the orbital occupations revealed either relative, weakly or semi-conducting properties, with a tendency towards insulating on increasing Co, with Fe and oxygen ions located between two Fe responsible for the tendency towards relative conduction, and Co and the oxygen ions located between two Co responsible for the tendency towards being insulating. Finally, we identified an intermediate state of Co and confirmed its hypothesized dependence on Co-O, d-p orbital hybridization, albeit in the presence of low spin Co.

This fundamental research into the effects of substituting $LaFeO_3$ with cobalt and the resulting properties of $LaCo_xFe_{1-x}O_3$ ($x \leq 0.5$) provides, in the first instance, atomistic detail for larger scale modelling, where, for example, we have shown that there are charge and spin differences between oxygen ions depending on their location. It also supplements the growing data bank of electronic structure results that provide subtle yet important detail to experimental results, see for example the interesting work of Gryaznov et al. [87] on the role of phonon contributions to oxygen vacancy formation energy (in $La_{1-x}Sr_xCo_{0.25}Fe_{0.75}O_{3-\delta}$). Given the vital role oxygen plays in the operation of SOFCs our next step is to use these results in larger scale models to determine in which way variously characterized oxygen ions and their vacancies behave differently.

Acknowledgements We would like to acknowledge the high performance computing (HPC) facilities in the Center for Computational Earth and Environmental Science (CEES) at Stanford University, and the Texas Advanced Computing Center (TACC), at the University of Texas at Austin for providing HPC resources that have contributed to the research results reported within this paper: URL: http://www.tacc.utexas.edu, as well as computing resources provided by STFC Scientific Computing Department's SCARF cluster.

References

[1] R. F. Savinell, Nature Chemistry 3, **501** (2011).
[2] R. Subbaraman, et al., Nature Materials **11**, 550 (2012).
[3] R. J. H. Voorhoeve, J. D. W. Johnson, J. P. Remeika, and P. K. Gallagher, Science **195**, 827 (1977).
[4] M. A. Peña and J. L. G. Fierro, Chem. Rev. **101**, 1981 (2001).

[5] Y.-L. Lee, D. Morgan, J. Kleis, and J. Rossmeisl, ECS Transactions **25**, 2761 (2009).
[6] J. Richter, P. Holtappels, T. Graule, T. Nakamura, and L. J. Gauckler, Monatsh Chem. **140**, 985 (2009).
[7] D. N. Mueller, M. L. Machala, H. Bluhm, and W. C. Chueh, Nature Comms. **6:6097**, 1 (2015).
[8] L. G. Tejuca and J. L. Fierro, Properties and Applications of Perovskite-Type Oxides (CRC Press, Taylor & Francis Group, 1992).
[9] L. G. Tejuca, J. L. Fierro, and J. M. D. Tascón, Advances in Catalysis (Academic Press, Elsevier B. V., 1989), p. 237.
[10] M. Johnsson and P. Lemmens, Crystallography and Chemistry of Perovskites, arXiv:cond-mat/0506606 (2005).
[11] S. P. Jiang, J. Mater. Sci. **43**, 6799 (2008).
[12] J. A. Kilner, A. Berenov, and J. Rossini, in Perovskite oxide for solid oxide fuel cells, edited by T. Ishihara, (Springer, 2009), p. 95.
[13] M. M. Kuklja, E. A. Kotomin, R. Merkle, Y. A. Mastrikov, and J. Maier, Phys. Chem. Chem. Phys. **15**, 5443 (2013).
[14] P. Kanhere and Z. Chen, Molecules **19**, 19995 (2014).
[15] Y.-L. Lee, J. Kleis, J. Rossmeisl, and D. Morgan, Phys. Rev. B **80**, 224101 (2009).
[16] Y.-L. Lee and D. Morgan, Phys. Chem. Chem. Phys. **14**, 290 (2012).
[17] M. T. Curnan and J. R. Kitchin, J. Chem. Phys. C 118, 28776 (2014).
[18] R. A. De Souza, M. S. Islam, and E. Ivers-Tiffée, J. Mater. Chem. **9**, 1621 (1999).
[19] A. M. Ritzmann, A. B. Muñoz-Garcia, M. Pavone, J. A. Keith, and E. A. Carter, MRS Communications **3**, 161 (2013).
[20] A. M. Ritzmann, A. B. Muñoz-Garcia, M. Pavone, J. A. Keith, and E. A. Carter, Chem. Mater. **25**, 3011 (2013).
[21] A. M. Ritzmann, M. Pavone, A. B. Muñoz-Garcia, J. A. Keith, and E. A. Carter, J. Materials Chemistry A **2,** 8060 (2014).
[22] S. M. Woodley, J. D. Gale, P. D. Battle, and C. R. A. Catlow, J. Chem. Phys. **119**, 9737 (2003).
[23] M. S. Islam, Solid State Ionics **75,** 154 (2002).
[24] A. B. Muñoz-Garcia, A. M. Ritzmann, M. Pavone, J. A. Keith, and E. A. Carter, Accounts of Chemical Research **47**, 3340 (2014).
[25] R. Merkle, Y. A. Mastrikov, E. A. Kotomin, M. M. Kuklja, and J. Maier, JECS Transactions **159**, B219 (2012).
[26] M. Pavone, A. M. Ritzmann, and E. A. Carter, Energy & Environmental Science **4**, 4933 (2011).
[27] M. Pavone, A. B. Muñoz-Garcia, A. M. Ritzmann, and E. A. Carter, J. Phys. Chem. C **118**, 13346 (2014).
[28] S. Ganopadhyay, T. Inerbaev, A. Masunov, D. Altilio, N. Orlovskaya, J. Mesit, R. Guha, A. Sleiti, and J. Kapat, in Fourth International Conference on MultiScale Material Modeling (MMM), Tallahassee, USA, 2008, p. 110.
[29] C. Chen, Z. M. Baiyee, and F. Ciucci, Phys. Chem. Chem. Phys. **17**, 24011 (2015).
[30] C. Chen, D. Chen, and F. Ciucci, Phys. Chem. Chem. Phys. **17**, 7831 (2015).
[31] Y. A. Mastrikov, R. Merkle, E. A. Kotomin, M. M. Kuklja, and J. Maier, Phys. Chem. Chem. Phys. **15**, 911 (2013).
[32] I. R. Shein, V. L. Kozhevnikov, and A. L. Ivanovskiĭ, J. Phys. Chem. Solids. **67**, 1436 (2006).
[33] I. Popescu, Y. Wu, P. Granger, and I.-C. Marcu, Applied Catalysis A: General **485**, 20 (2014).
[34] M. R. Goldwasser, M. E. Rivas, M. L. Lugo, E. Pietri, J. Pérez-Zurita, M. L. Cubeiro, A. Griboval-Constant, and G. Leclercq, Catalysis Today **107-108**, 106 (2005).
[35] Y. Wu, C. Cordier, E. Berrier, N. Nuns, C. Dujardin, and P. Granger, Applied Catalysis B: Environmental **140-141**, 151 (2013).
[36] S. Ivanova, A. Senyshyn, E. Zhecheva, K. Tenchev, R. Stoyanova, and H. Fuess, Journal of Solid State Chemistry **183**, 940 (2010).
[37] J. Bi, Y.-B. Wu, H.-Y. Zhao, and B.-B. Wei, Journal of Inorganic Materials **30**, 1031 (2015).
[38] M. M. Natile, F. Poletto, A. Galenda, A. Glisenti, T. Montini, L. D. Rogatis, and P. Fornasiero, Chem. Mater. **20**, 2314 (2008).
[39] S. I. Vecherskii, S. N. Tabatchikova, B. D. Antonov, and V. A. Biryukov, Inorganic Materials **47**, 1356 (2010).
[40] I. O. Troyanchuk, D. V. Karpinskiĭ, V. M. Dobryanskiĭ, Y. A. Fedotova, and H. Szymczak, J. Exper. Theoret. Phys. **100**, 1121 (2005).
[41] D. V. Karpinsky, I. O. Troyanchuk, K. Bärner, H. Szymczak, and M. Tovar, J. Phys. Condens. Matter **17**, 7219 (2005).
[42] H.-R. Fuh, K.-C. Weng, C.-R. Chang, and Y.-K. Wang, J. Applied Physics **117**, 17B902 (2015).
[43] S. J. Clark, M. D. Segall, C. J. Pickard, P. J. Hasnip, M. I. J. Probert, K. Refson, and M. C. Payne, Z. Kristallogr. **220**, 567 (2005).
[44] P. Hohenberg and W. Kohn, Phys. Rev. **136**, 864 (1964).
[45] W. Kohn and L. J. Sham, Phys. Rev. **140**, A1133 (1965).
[46] M. C. Payne, M. P. Teter, D. C. Allan, T. A. Arias, and J. D. Joannopoulous, Reviews of Modern Physics **64**, 1045 (1992).
[47] D. Vanderbilt, Phys. Rev. B **41**, 7892 (1990).
[48] G. Kresse and J. Hafner, J. Phys.: Condens. Matter **6**, 8245 (1994).
[49] S. G. Louie, S. Froyen, and M. L. Cohen, Phys. Rev. B **26**, 1738 (1982).
[50] J. P. Perdew, K. Burke, and M. Ernzerhof, Physical Review Letters **77**, 3865 (1996).
[51] B. G. Pfrommer, M. Côté, S. Louie, and M. L. Cohen, Journal of Computational Physics **131**, 233 (1997).
[52] N. Mazari, D. Vanderbilt, and M. C. Payne, Physical Review Letters **79**, 1337 (1997).
[53] H. J. Monkhorst and P. J.D., Phys. Rev. B **13**, 5188 (1976).
[54] G. Trimarchi and N. Binggeli, Phys. Rev. B **71**, 035101 (2005).
[55] I. Solovyev, N. Hamada, and K. Terakura, Phys. Rev. B **53**, 7158 (1996).
[56] S. K. Pandey, S. Khalid, and A. V. Pimpale, J. Phys.: Condens. Matter **19**, 036212 (2007).
[57] Z. Yang, Z. Huang, L. Ye, and X. Xie, Phys. Rev. B **60**, 15674 (1999).
[58] S. K. Pandey, A. Kumar, S. Patil, V. R. R. Medicherla, R. S. Singh, K. Maiti, D. Prabhakaran, A. T. Boothroyd, and A. V. Pimpale, Phys. Rev. B **77**, 045123 (2008).
[59] M. A. Korotin, S. Y. Ezhov, I. V. Solovyev, V. I. Anisimov, D. I. Khomskii, and G. A. Sawatzky, Phys. Rev. B **54**, 5309 (1996).
[60] N. J. Mosey, P. Liao, and E. A. Carter, J. Chem. Phys. **129**, 014103 (2008).
[61] N. J. Mosey and E. A. Carter, Phys. Rev. B **76**, 155123 (2007).

[62] J.-Q. Yan, J.-S. Zhou, and J. B. Goodenough, Phys. Rev. B **70**, 014402 (2004).
[63] W. C. Koehler and E. O. Wollan, J. Phys. Chem. Solids. **2**, 100 (1957).
[64] M. Abbate, J. C. Fuggle, A. Fujimori, L. H. Tjeng, C. T. Chen, R. Potze, G. A. Sawatzky, H. Eisaki, and S. Uchida, Phys. Rev. B **47**, 16124 (1993).
[65] R. S. Mulliken, J. Chem. Phys. **23**, 1833 (1955).
[66] W. Tang, E. Sanville, and G. Henkelman, J. Phys.: Condens. Matter **21**, 084204 (2009).
[67] E. Sanville, S. D. Kenny, R. Smith, and G. Henkelman, J. Comp. Chem. **28**, 899 (2007).
[68] G. Henkelman, A. Arnaldsson, and H. Jónsson, Comput. Mater. Sci. **36**, 254 (2006).
[69] D. Sanchez-Portal, E. Artacho, and J. M. Soler, Solid State Communications **95**, 685 (1995).
[70] R. S. Mulliken, J. Chem. Phys. **23**, 1841 (1955).
[71] R. S. Mulliken, J. Chem. Phys. **23**, 2338 (1955).
[72] R. S. Mulliken, J. Chem. Phys. **23**, 2343 (1955).
[73] M. D. Segall, C. J. Pickard, R. Shah, and M. C. Payne, Mol. Phys. **89**, 571 (1996).
[74] E. R. Davidson and S. Chakravorty, Theoret. Chim. Acta **83**, 319 (1992).
[75] J. Zaanen, G. A. Sawatzky, and J. W. Allen, Phys. Rev. Lett. **55**, 418 (1985).
[76] I. R. Shein, K. I. Shein, V. L. Kozhevnikov, and A. L. Ivanovskiĭ, Magnetism and Ferroelectricity **47**, 1998 (2005).
[77] D. Gryaznov, S. Baumann, E. A. Kotomin, and R. Merkle, J. Phys. Chem. C **118**, 29542 (2014).
[78] K. Tomiyasu, Y. Kubota, S. Shimomura, M. Onodera, S.-I. Koyama, T. Nojima, S. Ishihara, H. Nakao, and Y. Murakami, Phys. Rev. B **87**, 2244091 (2013).
[79] M. M. Kuklja, Y. A. Mastrikov, B. Jansang, and E. A. Kotomin, J. Phys. Chem. C **116**, 18605 (2012).
[80] A. Weizman, D. Fuks, E. A. Kotomin, and D. Gryaznov, Solid State Ionics **230**, 32 (2013).
[81] D. Fuks, Y. Mastrikov, E. Kotomin, and J. Maier, J. Mater. Chem. A **1**, 14320 (2013).
[82] G. Kresse and D. Joubert, Phys. Rev. B **59**, 1758 (1999).
[83] E. G. Moroni, G. Kresse, and J. Hafner, Phys. Rev. B **56**, 15629 (1997).
[84] J. Heyd, G. E. Scuseria, and M. Ernzerhof, J. Chem. Phys. **118**, 8207 (2003).
[85] J. Heyd, G. E. Scuseria, and M. Ernzerhof, J. Chem. Phys. **124**, 219906 (2006).
[86] F. El-Mellouhi, E. N. Brothers, M. J. Lucero, I. W. Bulik, and G. E. Scuseria, Phys. Rev. B **87**, 035107 (2013).
[87] D. Gryaznov, M. W. Finnis, R. A. Evarestov, and J. Maier, Solid State Ionics **254**, 11 (2014).